East European Journal of Physics. 2. 541-553 (2026)
DOI:10.26565/2312-4334-2026-2-61 ISSN 2312-4334

ESTIMATION OF THE GAMMA EXPOSER RATE CONSTANT FOR CLINICALLY RELEVANT RADIONUCLIDES IN NUCLEAR MEDICINE USING GATE/GEANT4 MONTE CARLO SIMULATION

Abdulkhaleq O. Jaralah[1], Alaa M. Elgohary[1], Monira M. Rageh[1], Magdy M. Khalil[2,3]
[1]*Department of Biophysics, Faculty of Science, Cairo University, Egypt*
[2]*Medical Biophysics, Department of Physics, Faculty of Science, Helwan University*
[3]*School of Applied Health Sciences, Badr University in Cairo (BUC), Cairo, Egypt*
**Corresponding Author E-mail: magdy_khalil@hotmail.com*
Received March 4, 2026; revised April 15, 2026; accepted May 20, 2026

Purpose. To establish a reliable computational method for calculating external radiation dose rates from nuclear medicine patients using Monte Carlo simulation and to systematically evaluate the effects of phantom geometry and detector characteristics on occupational exposure. **Methods:** MC GATE simulations version 9.1 (Geant4 10.7) calculated external dose rate constants for most clinical radionuclides: ^{99m}Tc, ^{67}Ga, ^{18}F, ^{11}C, ^{131}I, and ^{123}I. Two phantoms were used, one with dimensions of (25×15×20, 30×20×25, and 35×25×30 cm^3), and the other with a fixed length of 170 cm and variable width (15×20, 20×25, and 25×30 cm^3), specific to the ^{99m}Tc nuclide. Detector sizes (3×3×3 to 10×10×10 cm^3) were evaluated at distances of 1, 2, and 3 m. Different detector media (air, argon, and neon) were assessed for photon sensitivity. The results were compared with experimental data. **Results:** Simulated results agreed with experimental data within ±10%. Argon demonstrated superior sensitivity compared with air and neon detector media. Phantom dimensions increased overall, resulting in a 36.8% reduction due to self-attenuation. Radionuclides of ^{18}F and ^{11}C, followed by ^{67}Ga, ^{131}I, ^{123}I, and ^{99m}Tc, posed the highest occupational exposure hazard. Patient body thickness was a more significant attenuation factor than patient height. **Conclusion:** GATE/Geant4 simulations provide a reliable and accurate tool for evaluating external dose rates in nuclear medicine departments. These findings underscore the importance of using appropriate detector sizes and media, as well as realistic patient geometry, in occupational dose assessments and provide essential data to improve radiation protection protocols.
Keywords: *External dose rate; Nuclear Medicine; Radiation Protection; Monte Carlo simulation; Gamma rate constant*
PACS: 02.70.Uu, 07.05Tp

1. INTRODUCTION

Nuclear medicine is an important medical specialty that uses radioactive substances for diagnostic and therapeutic procedures [1]. Fluorodeoxyglucose (F18-FDG) has a specific role in clinical oncology for patient stratification, diagnosis, staging, restaging, and management [2]. Technetium (^{99m}Tc) is the workhorse of most nuclear medicine examinations in the diagnosis of many diseases, including orthopedic, cardiac, urological, endocrine, and other pathologies [1]. Gallium-67 (67Ga) has been used to image inflammation and infection, as well as various solid neoplasms, particularly lymphomas [3].

An iodine-131 (131I) and iodine-123 (^{123}I) nuclide scan is a noninvasive imaging procedure used to detect metastatic thyroid cancer and assess the remaining thyroid tissue after thyroidectomy and thyroid cancer treatments [4,5]. The carbon-11 (^{11}C) nuclide makes an ideal non-invasive option for targeted labeling molecules in PET imaging [6].

After patients are injected with radiopharmaceuticals, they become a source of contamination, emitting ionizing radiation to those who come into contact with them [7].

Each radiation exposure in nuclear medicine, even if minimal, potentially carries an inherent risk. This risk, primarily the potential for genetic alterations or malignancies, requires careful use of radionuclides by medical staff when administering pharmaceuticals [8].

The reduction of occupational exposure is by the ALARA acronym, which stands for "As Low As Reasonably Achievable" principles, optimizing dose in any work that includes radiation exposure. This crucial endeavor in radiation safety helps reduce occupational exposure. ALARA encapsulates the obligation to avoid unnecessary radiation exposure, emphasizing that any exposure should be clinically indicated and provide a direct benefit to the ALARA principles, which manifest through three essential strategies (Time, Distance, Shielding), each designed to reduce radiation exposure consistently, which are dependent on precise dose rate [9]. The exposure dose rate constant (Γ) is essential in dosimetry for estimating dose rate at distance (usually at 1 m from the source) to ensure a safe environment and monitoring, by ICRP and IAEA [10,11]

The International Commission on Radiological Protection (ICRP) has established a radiation dose rate of 20 μSv h^{-1} at a distance of 1m from the patient as one of the criteria for discharging patients after injection with radioactive isotopes [12].

Some researchers have adopted a dose calculation method whereby radioactivity within the patient, as a point source, is subject to the inverse-square law, and the physical half-life is taken into account instead of the effective half-life [13,14].

Cite as: A.O. Jaralah, A.M. Elgohary, M.M. Rageh, M.M. Khalil, East Eur. J. Phys. 2, 541 (2026), https://doi.org/10.26565/2312-4334-2026-2-61

Monte Carlo simulation has emerged as a prominent tool in radiation protection and dosimetry, capable of simulating complex scenarios that are otherwise infeasible due to ethical or spatial constraints. One such Monte Carlo simulation platform, specializing in nuclear medicine, is GATE (GEANT4 Application to Tomographic Emission). Based on the Geant4 (GEometry ANd Tracking) libraries, it offers a scripting interface with numerous advantages for simulating SPECT and PET systems. It boasts high performance in measuring internal and external radiation doses [15].

Despite previous studies investigating external radiation exposure from nuclear medicine patients using MCNP simulation, a clear lack of understanding persists. Simple geometry was used to calculate dose rates, employing a point source without any attenuation to ensure realism. This leads to significant overestimation of dose rates, especially at short distances. While some studies have suggested simulating linear or point sources to improve exposure accuracy, systematic evaluation of the impact of patient dimensions, such as thickness and height, remains limited [15,16]. In the Soares et al. 2018 study, which used MCNPX and employed anthropomorphic voxel phantoms based on ICRP-110, although the study was comprehensive, it did not assess the dose rate on the effect of anatomical differences, such as variations in height and width [18].

This focused on the need to use Monte Carlo simulation to assess the impact of phantom geometry and varying distances between the source and detector, comparing dose rates between the bare source and the phantom to better support radiation protection and enhance the safety of workers and the public.

This study aimed to use the Geant4/Gate Monte Carlo simulation to calculate dose rates for most radionuclides employed in nuclear medicine by systematically varying phantom dimensions and detector-phantom distances, and employing different detector media (air, argon, and neon) to evaluate detector media and responses on dose rate values.

2. MODELING AND METHODS

2.1 GATE simulation setup

The simulations were performed using GATE (version 9.1) installed in combination with Geant4 (version 10.7) [19]. The simulation was run on an HP laptop with an Intel Core i5-7Y54 processor and 8 GB of RAM. The GATE was operated on an Ubuntu Oracle virtual machine hosted on a Windows 10 Pro operating system.

2.2 World Geometry

In the MC GATE simulation, a cubic environment with equal dimensions of 6×6×6 m^3 was created and filled with air, as specified in the GateMaterials database. These dimensions were chosen to ensure accurate and complete containment and tracking of primary and secondary particles, thereby enabling accurate analysis of energy distribution across the entire simulation domain and eliminating boundary-related photon-scattering artifacts that affect dose calculation accuracy.

2.3 Physics List

The physics list was used in this simulation, and all electromagnetic interactions involving transport particles and photons are consistent with those of the radionuclide used in nuclear medicine. Regarding photon transport, Compton scattering and the photoelectric effect were implemented, and Rayleigh scattering was implemented using the Penelope model [11]. Charged-particle interactions, positron and electron decays, bremsstrahlung, and high-energy annihilation (511 keV) were also implemented. A physics list for radioactive decay was also used to accurately simulate this process, resulting in the emission of gamma rays [20]. This approach ensures the optimal balance between dose recorder accuracy and computational efficiency.

2.4 Phantom Geometry and Dimension

In this study, a water-based phantom with a water density of 1.0 g/cm^3, equivalent to human soft tissue, was used. The phantom was modeled using geometric shapes with varying length and width to assess changes in external exposure across different phantom dimensions. Two sets of phantom configurations were used in this study. The first set of phantoms, based on the ICRP-110 report for the adult voxel phantom, has a height of 176 cm for males and 168 cm for females.

In this work, the mean ICRP-110 report tall phantom, with a fixed height of 170 cm and variable width (15×20, 20×25, and 25×30 cm^3), was used to ensure optimal assessment of the external radiation dose rate. This largely simulated the variable dimensions of the human thorax. The second set of phantoms had smaller overall dimensions (25×15×20, 30×20×25, and 35×25×30 cm^3). The phantom dimensions were derived from the transverse thoracic diameter of an adult Nigerian population [20].

However, the effect of varying the phantom length and width on the external dose rate was evaluated under the same radiation conditions. A point source was placed inside the phantom at a predetermined position. Using a point source enables precise calculations and facilitates the evaluation of how variations in geometric shape affect the dose rate.

2.5 Source Configuration

In this study, the source was modeled as a point source and defined as an ion source with isotropic emission in all directions, using a general particle source (GPS). The point source emits particles and photons of each radionuclide according to the physics decay scheme. Fluorine-18 and Carbon-11, the positron-emitting radionuclides, undergo β^+

decay, producing positrons and neutrinos, which generate two gamma photons with an energy of 511 keV. In contrast, Iodine-123 emits gamma photons with an energy of 159 keV. Iodine-131 emits beta particles accompanied by gamma photons at 364 keV.

Gallium-67 decays by electron capture and emits photons with energies around 93, 184, and 300 keV. Technetium-99m emits a gamma photon with an energy of 140 keV [1]. The source was placed in two conditions: in the first, it was an unshielded source to ensure the absence of Compton scattering or attenuation that might absorb a portion of the photons, and to calculate an external dose rate constant (Γ) to be used as a reference and compared with previous studies.

In the second, the source was placed inside the phantom to calculate the dose and determine the extent to which self-attenuation and scattering affect radiation exposure under realistic clinical conditions. The radioactivity used in the simulation was 100 kBq for an acquisition time of 60 s to produce 6×10^6 particle histories. This event number was used in the simulation to ensure the statistical uncertainties in the dose rate values, resulting in a maximum relative standard deviation of 1.5%.

2.6 Detector Geometry and Dose Calculation

A detector was modeled to measure radiation exposure. The detector was designed to operate with different gaseous media: air, argon, and neon. Each gas detector was assigned to a specific boundary, and its physical properties were specified. The densities of air, argon, and neon were set to 1.22×10^{-3} g/cm³, 1.61×10^{-3} g/cm³, and 8.39×10^{-4} g/cm³, with effective atomic numbers Zeff ≈ 7.6, Z = 18, and Z = 10, respectively.

The purpose of this study was to examine the effect of gas type on photon energy deposition. The detector was placed at distances of 1, 2, and 3 m from the source to evaluate the effect of distance on the external radiation dose. The detector size was varied from (3×3×3 cm³ to 10×10×10 cm³) to assess the measurement response and the accuracy of dose calculation. The detector was coupled within a Geant4 Gate simulation with a Dose Actor to calculate photon energy deposition within the detector volume. The effect of low-energy interactions, which are not scientifically significant at doses below 10 keV, was neglected to ensure high consistency with previous studies, including Unger & Trubey (1982) [21]. In the dose actor, the energy of the deposit was converted into a radiation dose according to the following equation:

$$D = \frac{E_{dep}}{m} \quad (1)$$

Where D represents the absorbed dose (Gy), E_{dep} is the energy deposited within the detector volume (J), and m is the detector mass (kg), calculated using the previously defined detector volume and density [22].

3. RESULTS

3.1 Unshielded point source

Figure 1 shows six separate graphs (a-f) comparing dose-rate constant values from GATE/Geant4 simulations with previous experimental studies for the six nuclides across different detector media (air, argon, neon) and multiple detector sizes at 1 m from an unshielded point source.

Table 1 shows a comparison of GATE simulations using different detector dimensions and gas media with published data. The optimal detector size that gave results closest to experimental values was selected. The matching results showed variation in the detector dimensions and media depending on the specific radionuclide; the agreement ratio was calculated between the simulation and published data, and the deviation was within ±10% of the total experimental data. In the study by Unger & Trubey (1982) [21], the mean overall agreement ratio and standard deviation (SD) were 1.089±0.120, in the study by Tschurlovits et al. (1992) [23], it was 1.127±0.194, and in the study by Smith & Stabin (2012), it was 1.114±0.241[24].

Table 1. Validation of the MC Gate simulation of dose rate constants for radionuclides with experimental published previous studies at 1 m.

Nuclide	Experimental		Simulation			Ratio
	Reference	Γ (mSv·m²/MBq·h)	Detector Size (cm³)	Media Detector	Γ (mSv·m²/MBq·h)	
^{11}C	Unger & Trubey (1982)	1.91×10^{-4}	8×8×8	Argon	1.86×10^{-4}	0.973
	Tschurlovits et al. (1992)	1.39×10^{-4}	9×9×9	Air	1.36×10^{-4}	0.978
	Smith & Stabin (2012)	1.54×10^{-4}	7×7×7	Argon	1.66×10^{-4}	1.078

Nuclide	Experimental		Simulation			Ratio
	Reference	Γ (mSv·m²/MBq·h)	Detector Size (cm³)	Media Detector	Γ (mSv·m²/MBq·h)	
^{18}F	Unger & Trubey (1982)	1.85×10^{-4}	6×6×6	Argon	1.77×10^{-4}	0.956
	Tschurlovits et al. (1992)	1.37×10^{-4}	8×8×8	Air	1.40×10^{-4}	1.022
	Smith & Stabin (2012)	1.49×10^{-4}	10×10×10	Argon	1.49×10^{-4}	1.000
^{67}Ga	Unger & Trubey (1982)	3.00×10^{-5}	9×9×9	Argon	3.57×10^{-5}	1.190
	Tschurlovits et al. (1992)	3.10×10^{-4}	4×4×4	Argon	3.42×10^{-4}	1.103
	Smith & Stabin (2012)	2.08×10^{-5}	9×9×9	Neon	2.02×10^{-5}	0.971
^{123}I	Unger & Trubey (1982)	7.48×10^{-5}	7×7×7	Air	9.21×10^{-5}	1.231
	Tschurlovits et al. (1992)	1.69×10^{-4}	10×10×10	Argon	1.93×10^{-4}	1.142
	Smith & Stabin (2012)	4.54×10^{-5}	10×10×10	Air	4.14×10^{-5}	0.912
^{131}I	Unger & Trubey (1982)	7.64×10^{-5}	6×6×6	Argon	8.91×10^{-5}	1.166
	Tschurlovits et al. (1992)	5.93×10^{-5}	6×6×6	Argon	8.91×10^{-5}	1.503
	Smith & Stabin (2012)	5.65×10^{-5}	6×6×6	Argon	8.91×10^{-5}	1.577
^{99m}Tc	Unger & Trubey (1982)	3.32×10^{-5}	9×9×9	Argon	3.39×10^{-5}	1.021
	Tschurlovits et al. (1992)	3.60×10^{-5}	6×6×6	Argon	3.66×10^{-5}	1.017
	Smith & Stabin (2012)	2.06×10^{-5}	4×4×4	Argon	2.36×10^{-5}	1.146

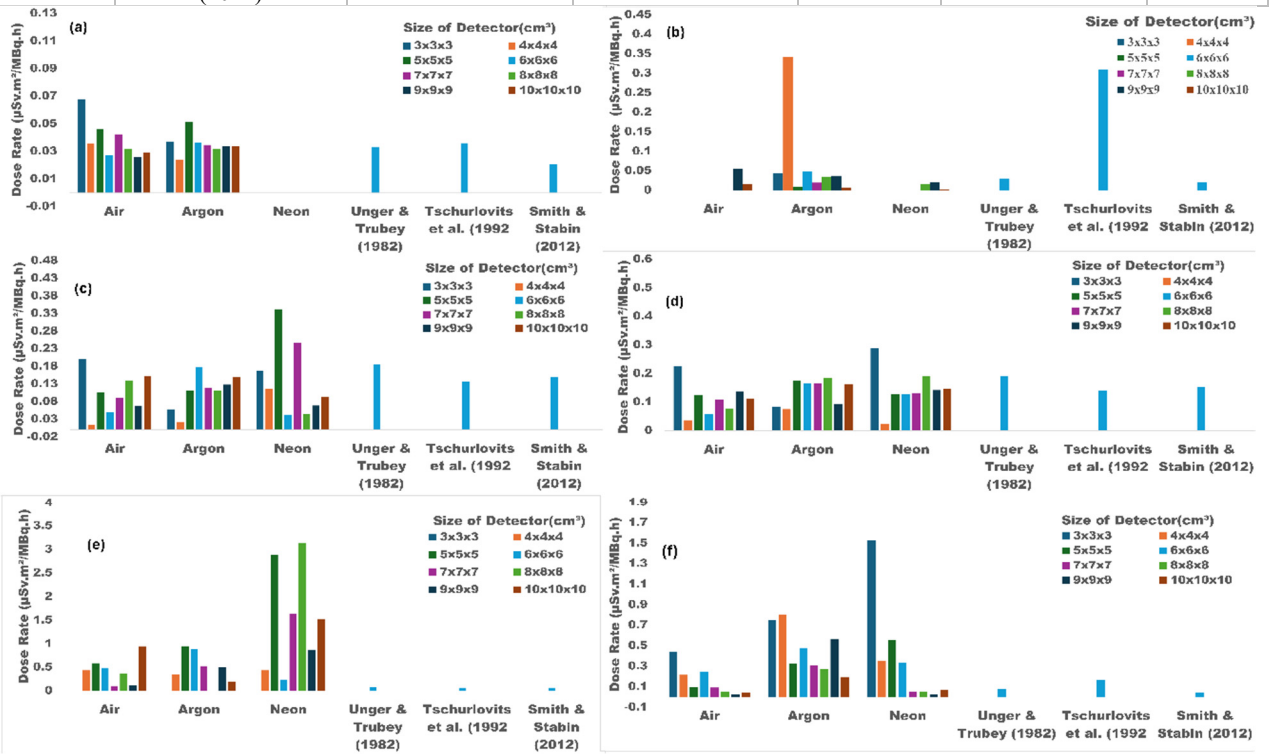

Figure 1. Simulation of external dose rate constants for (a) ^{99m}Tc, (b) ^{67}Ga, (c) ^{18}F, (d) ^{11}C, (e) ^{131}I, and (f) ^{123}I radionuclides in various detector media and different detector sizes, compared to previous studies at 1 m from an unshielded point source

The six nuclides used in the present work and investigated in different media (air, argon, and neon) are shown in Figure 2. The figure presents the mean external dose rate constant values for an unshielded point source isotropic emission, for detector sizes ranging from (8×8×8 to 10×10×10 cm^3). These values were compared with those from previous experimental studies that used an unshielded bare point source at 1m.

The results showed a dose rate constant of 0.0108 $\mu Sv \cdot m^2 \cdot MBq^{-1} \cdot h^{-1}$ in air detector media for ^{99m}Tc, a higher dose rate of 0.0418 $\mu Sv \cdot m^2 \cdot MBq^{-1} \cdot h^{-1}$ for argon detector media, the neon detector media failed to record a reading, unlike the air and argon detector media, which showed a perfect balance between the simulation results and previous reference studies.

In the ^{131}I, the highest reading was recorded in neon at 0.840 $\mu Sv.m^2. MBq^{-1}.h^{-1}$, indicating the neon detector media high sensitivity to radionuclides that have multiple energies. ^{131}I recorded high values in the neon detector, exceeding those of the air and argon detectors. The ^{123}I nuclide in the argon detector media showed a higher response than in air and neon, consistent with the study conducted by Tschurlovits et al. in 1992 [23]. As for the ^{67}Ga nuclide, the study by Tschurlovits et al. 1992 [23] stands out as a high value compared to other studies of different detector media simulations.

Conversely, for ^{18}F and ^{11}C nuclides, there is significant agreement and stability in the different detector media with the results of previous studies. The ratio agreement between the simulation and experiment published data for ^{18}F showed the argon media 0.70,0.94, and 0.87 for Unger & Trubey (1982) [21], Tschurlovits et al. (1992) [23], and Smith & Stabin (2012) [24], respectively, and air media was 0.70,0.88, and 0.81 for Unger & Trubey (1982) [21], Tschurlovits et al. (1992) [23], and Smith & Stabin (2012) [24] , respectively, and neon media was 0.40,0.55, and 0.46.for Unger & Trubey (1982) [21], Tschurlovits et al. (1992) [23], and Smith & Stabin (2012) [24], respectively.

Followed by the ^{11}C nuclide, the argon media 0.77,1.06, and 0.96 for Unger & Trubey (1982) [21], Tschurlovits et al. (1992) [23], and Smith & Stabin (2012) [24], respectively. and the air media was 0.60,0.80, and 70 for Unger & Trubey (1982) [21], Tschurlovits et al. (1992) [23], and Smith & Stabin (2012) [24], respectively, while the neon media were 0.90,1.16, and for 0.84 Unger & Trubey (1982) [21], Tschurlovits et al. (1992) [23], and Smith & Stabin (2012) [24], respectively.

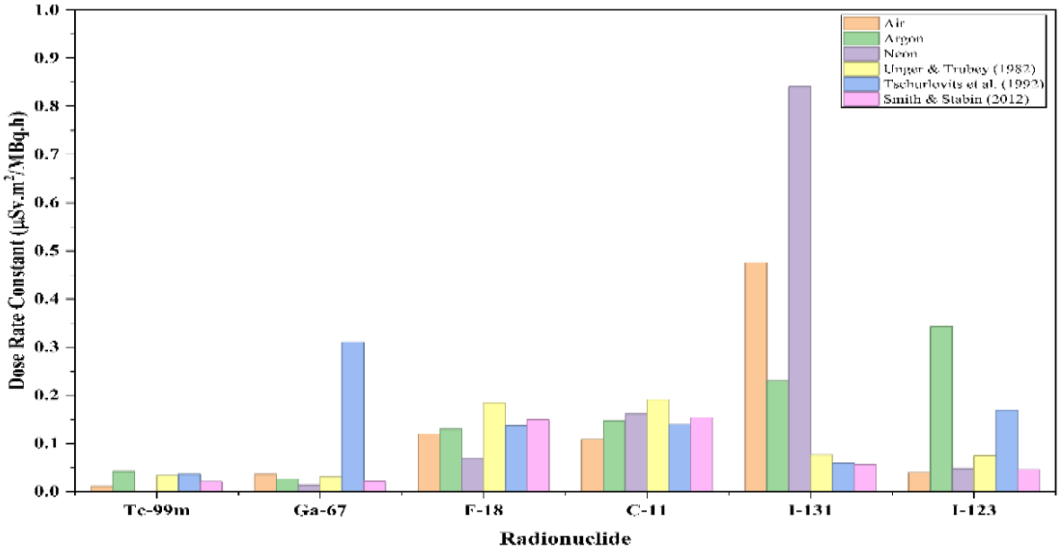

Figure 2. Mean dose rate constants for radionuclides in various detector media and different detector sizes (from 8×8×8 to 10×10×10 cm^3) at 1 m

3.2 Phantom Measurements (Shielded Source)

Figures (3, 4, 5) illustrate the effects of variations in phantom dimensions, detector size, and media (air, argon, and neon) on the dose rate constant. Variable phantoms measuring (25×15×20 cm^3, 30×20×25 cm^3, and 35×25×30 cm^3) were used, with detector sizes ranging from (3×3×3 cm^3 to 10×10×10 cm^3) at 1 m, compared with previous studies. Variations were measured from the initial valid readings to the 10×10×10 cm^3 detector size for each radionuclide.

Figure 3. (air detector media), ^{99m}Tc with variations of 78.3%, 94%, and 60% and ^{67}Ga recorded decreases of 69.4% and 47.7% and 81.9%, ^{18}F with variations of 35.1%, 47.1%, and 54.7%, ^{11}C and ^{131}I showed decreases for the small phantom (61.5% and 51.1%, respectively) but highly irregular increases for the larger phantoms, and ^{123}I with variations of 3.1%, 83.9%, and 99.8% for all the small, medium, and large phantoms, respectively.

Figure 4 (argon detector media) shows the same general pattern of decrease with phantom size, but with significantly higher dose rate values than the air media detector, with ^{99m}Tc 23.3% and 35% and 30.1%, ^{67}Ga with variations of 59.9%, 61.7%, and 60.3%, and ^{18}F showed variations of 10.9%, 90.5%, and 61.7%, ^{11}C recorded variations with decreases of 52.6%,5.3% and,12.1%and ^{131}I demonstrated variations of 142.0%, 151.8%, and 108.0%, and ^{123}I with variations 2.3%, 13.9%, and 17.3% for all the small, medium, and large phantoms, respectively.

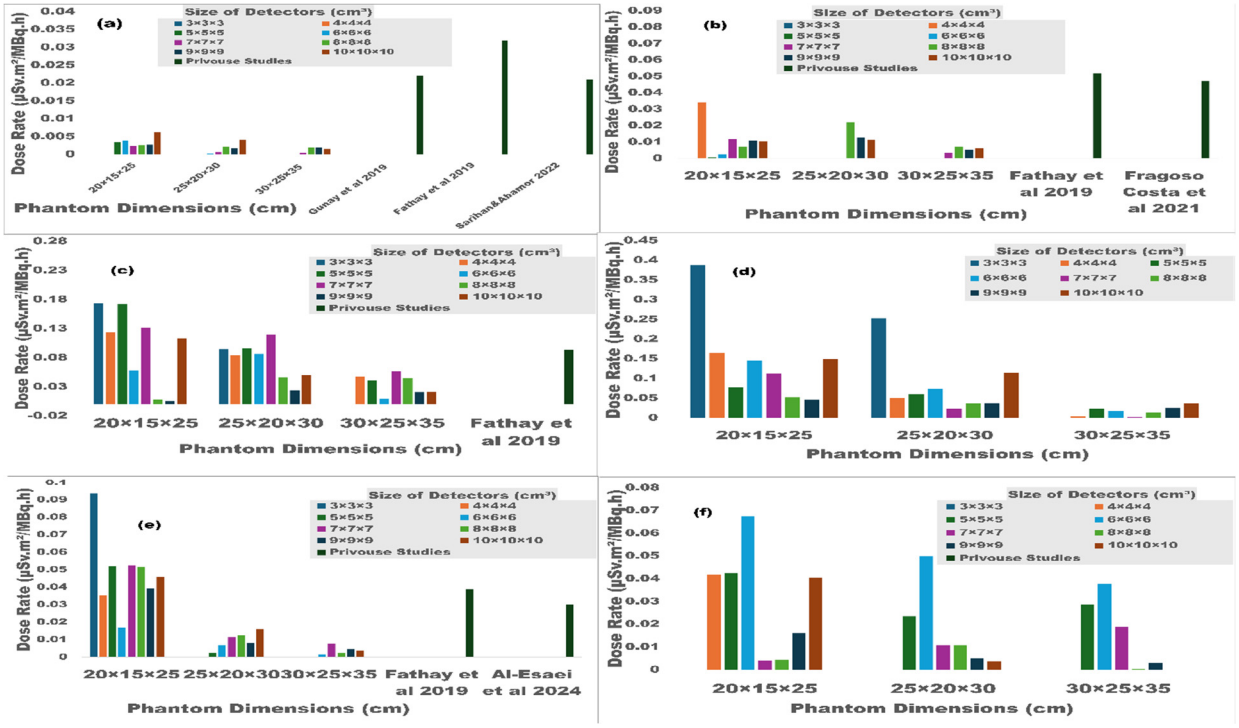

Figure 3. Simulation of external dose rate for (a)^{99m}Tc, (b) ^{67}Ga, (c) ^{18}F, (d) ^{11}C, (e) ^{131}I, and (f) ^{123}I radionuclides in air detector media and different phantom dimensions and detector sizes, compared to previous studies at 1 m.

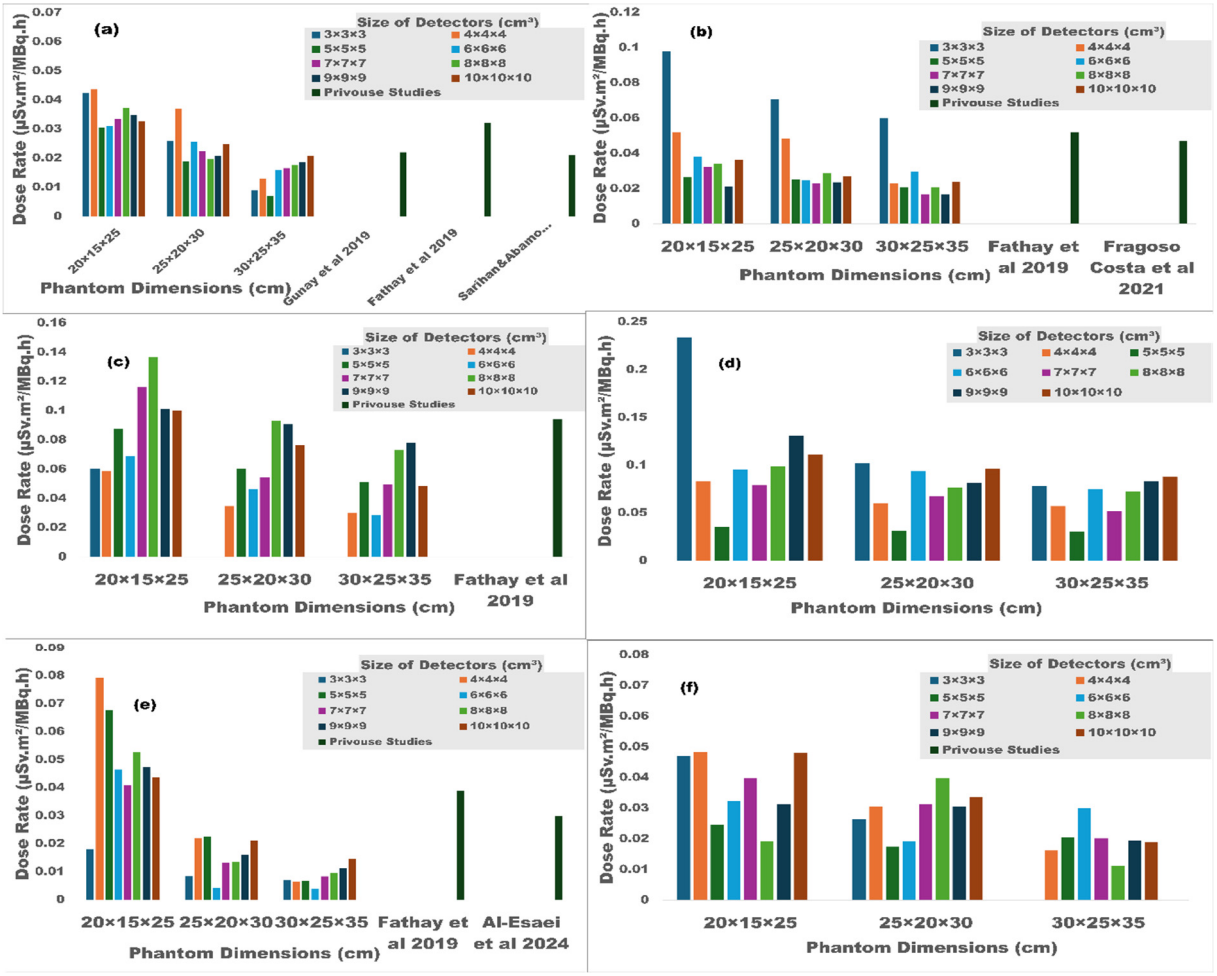

Figure 4. Simulation of external dose rate for (a)^{99m}Tc, (b) ^{67}Ga, (c) ^{18}F, (d) ^{11}C, (e) ^{131}I, and (f) ^{123}I radionuclides in argon detector media and different phantom dimensions and detector sizes, compared to previous studies at 1 m

Figure 5 (neon detector media) shows exhibited highly irregular behavior where ^{99m}Tc failed to register any measurable readings across all detector sizes and phantom dimensions, and ^{123}I failed to record large phantom(30×25×35 cm^3), ^{123}I recorded variations of 47.2% and 25.0% for the small and medium phantoms only, ^{67}Ga recorded with variations of 76.7%, 58.7%, and 92.3%, ^{131}I exhibited an increasing trend with variations of 73.4%, 50.5%, and 9.6%, and ^{11}C showed consistent decreasing trends of 41.5%, 34.6%, and 79.8%, ^{18}F showed variations of 31.7%, 91.2%, and 3.9%. for all the small, medium, and large phantoms, respectively,

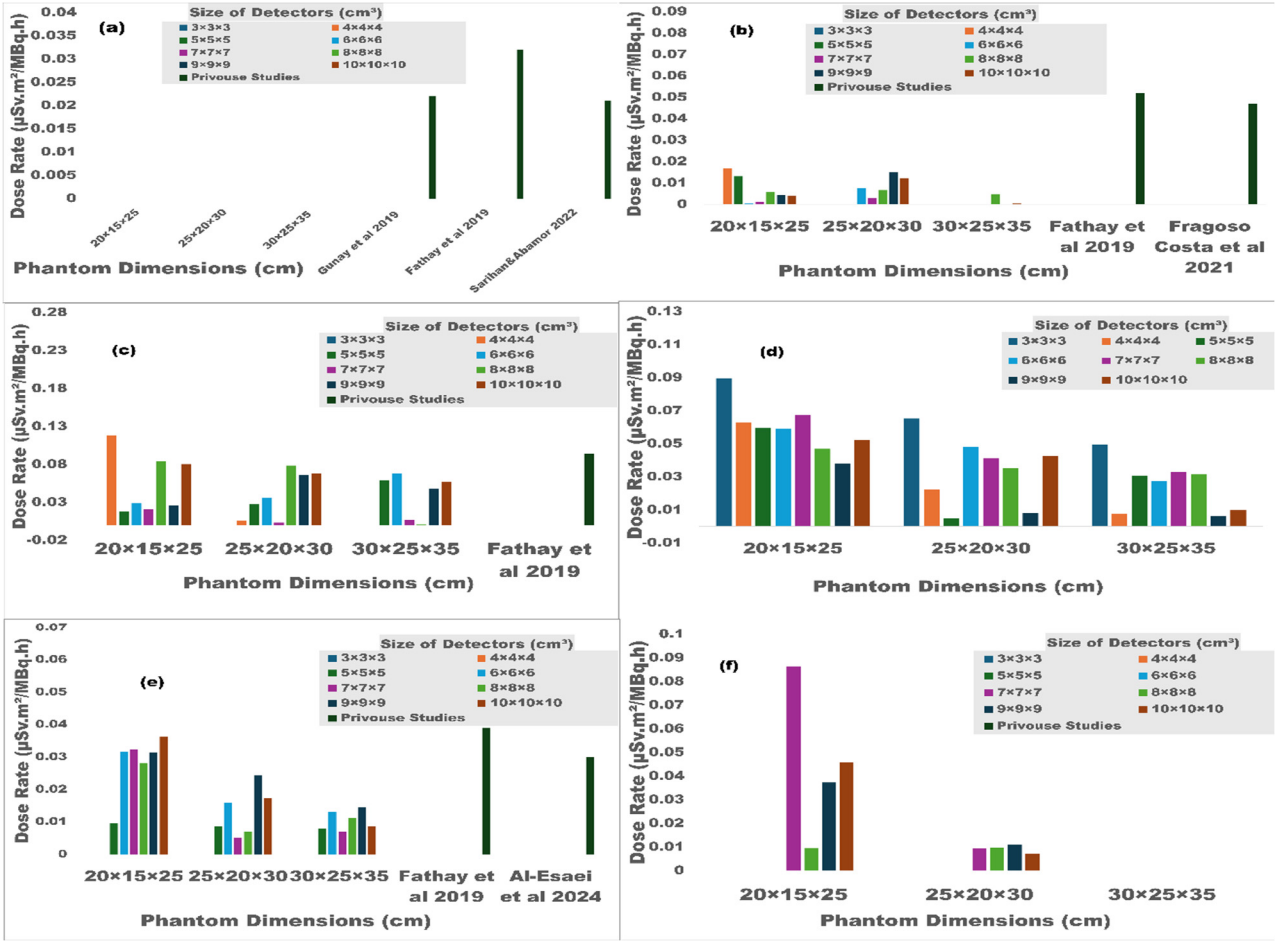

Figure 5. Simulation of external dose rate for (a)^{99m}Tc, (b) ^{67}Ga, (c) ^{18}F, (d) ^{11}C, (e) ^{131}I, and (f) ^{123}I radionuclides in Neon detector media and different phantom dimensions and detector sizes, compared to previous studies at 1 m.

Figure 6 presents three sets (a, b, c) showing the mean dose rates of the six radionuclides in the three-detector media (air, argon, and neon) across different phantom dimensions (25×15×20 cm^3, 30×20×25 cm^3, and 35×25×30 cm^3) and compares them with previous experimental studies.

In set (a) for the air detector media, ^{99m}Tc decreases from 0.0038 to 0.0019 μSv·m^2 (50% reduction), and ^{67}Ga decreases from 0.0125 to 0.0062 μSv·m^2·MBq^{-1}·h^{-1} (50% reduction), ^{18}F decreases from 0.0423 to 0.0211 μSv·m^2. MBq^{-1}·h^{-1} (50% reduction), and ^{11}C decreased from 0.0389 to 0.0254 μSv·m^2·MBq^{-1}·h^{-1} (35% reduction), ^{131}I decreased from 0.0318 to 0.0114 (64% reduction), and ^{123}I decreased from 0.0136 to 0.0011 μSv·m^2·MBq^{-1}·h^{-1} (92% reduction).

In set (b), the argon detector shows the same general pattern of decrease with phantom size, but with significantly higher dose rate values than the air media detector, with ^{99m}Tc increasing from 0.0349 μSv·m^2·MBq^{-1}·h^{-1} to 0.0218 μSv·m^2. MBq^{-1}·h^{-1} (37% reduction), ^{67}Ga increasing from 0.0420 to 0.0307 μSv·m^2 MBq^{-1}·h^{-1} (27% reduction), and ^{18}F rises from 0.0950 to 0.0760 μSv·m^2·MBq^{-1}·h^{-1} (20% reduction), ^{11}C rises from 0.0776 to 0.0564 μSv·m^2· MBq^{-1}·h^{-1} (27% reduction), ^{131}I decreases from 0.0478 to 0.0118 μSv·m^2·MBq^{-1}.h^{-1} (a 75% reductions), and ^{123}I decreases from 0.0362 to 0.0166 μSv·m^2·MBq^{-1}·h^{-1} (a 54% reductions).

In set (c), the neon media shows irregular, more complex, and inconsistent behavior where ^{99m}Tc and ^{123}I record very low or nearly zero values, and ^{123}I decreases from 0.0309 to 0.00 in the larger phantom, while ^{67}Ga rises to 0.0165 μSv.m^2. MBq^{-1}·h^{-1} and falls to 0.0017 μSv·m^2·MBq^{-1}·h^{-1} (90% reduction), and ^{131}I records the highest absolute value ever of 0.8407 μSv·m^2·MBq^{-1}·h^{-1} but drops sharply to 0.0035 (99% reductions), and ^{11}C rises to 0.1607 μSv·m^2·MBq^{-1}·h^{-1} and falls to 0.0293 μSv·m^2 (81% reductions). MBq^{-1}·h^{-1}, and ^{18}F rises to 0.0733 and falls to 0.0453 μSv·m^2·MBq^{-1}·h^{-1} (38.2% reductions).

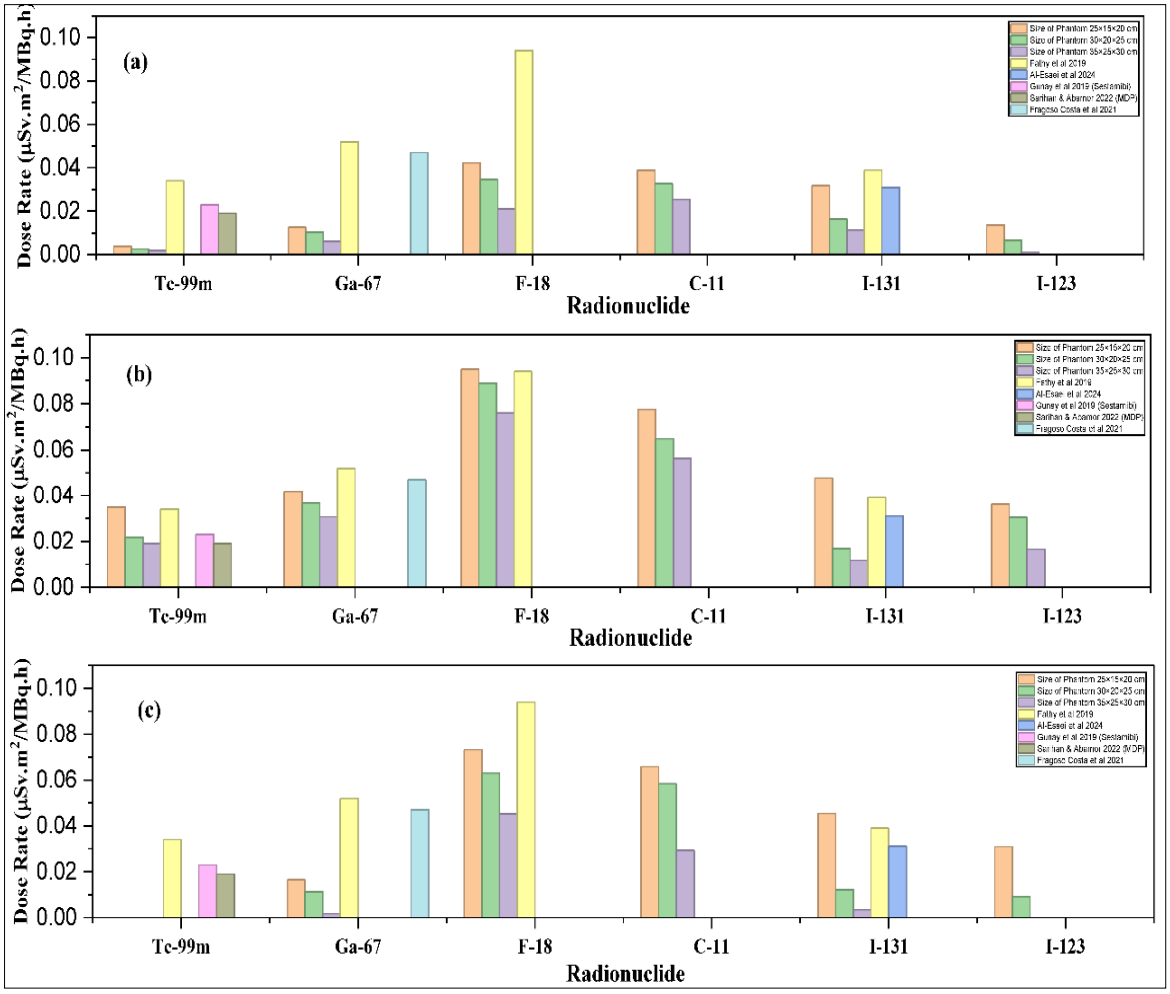

Figure 6. Mean dose rate constant for the radionuclides used, (a) air, (b) argon, and (c) neon detector media for detector size (from 8×8×8 to 10×10×10 cm^3) with different phantom dimensions, compared with previous studies at 1 m

Figure 7 (a and b) describes the ^{99m}Tc nuclide, comparing the dose rate across two different detector media (air and argon) and the two sets of phantoms. Where the dimensions were divided into small (170×15×20 and 25×15×20 cm^3), medium (170×20×25 and 30×20×25 cm^3), and large phantoms (170×25×30 and 35×25×30 cm^3) at 1 m compared with previous studies.

Figure (7a), which represents air detector media, the GATE simulation values are very low, starting at 0.0038 μSv·m²·MBq^{-1}·h^{-1} for the small phantom and gradually decreasing to 0.0026 μSv·m²·MBq^{-1}·h^{-1} for the medium phantom (a 31.6% reductions), then to 0.0019 μSv.m². MBq^{-1}.h^{-1} for the large phantom (50% reductions).

Figure (7b), which represents argon detector media, shows much better agreement, with GATE simulation values starting at 0.0349 μSv·m²·MBq^{-1}·h^{-1} for the small phantom, but decreasing to 0.0218 μSv·m²·MBq^{-1}·h^{-1} for the medium phantom (37.5% reductions), and then to 0.0191 μSv·m²·MBq^{-1}·h^{-1} for the large phantom (12.4% reductions). (Supplement file shows the ^{99m}Tc nuclide used with an argon detector media for various phantoms and detector sizes at 1, 2, 3 m with previous studies in Figure S1 to Figure S3).

Table 2 presents the results for the ^{99m}Tc nuclide, demonstrating that the dose rates recorded conform to the inverse-square law across different phantom dimensions, and selected optimal detector sizes prove the inverse-square law.

The argon detector media maintained its ability to produce measurable readings at 1, 2, and 3 m, whilst the air and neon detectors failed. The power-law fitting function, whilst the exponential coefficient 1/r² presents a range from −0.167 to −1.054 across all phantom dimensions, deviating from the ideal value -2 of the inverse-square law for an unshielded point source. (Supplement file shows Figure S4 to Figure S11)

Table 2. Analysis of the Inverse-Square Law distances of 1, 2, and 3 m from the source across various phantom dimensions and detector sizes for the ^{99m}Tc nuclide.

Phantom Dimension (cm^3)	Size of the Detector (cm^3)	Fitting Function	R^2	$1/r^2$
170×15×20	10×10×10	$y=0.0300x^{-0.258}$	0.9760	-0.258
	9×9×9	$y=0.0285x^{-0.293}$	0.8646	-0.293
	8×8×8	$y=0.0335x^{-0.483}$	0.9836	-0.483

Phantom Dimension (cm^3)	Size of the Detector (cm^3)	Fitting Function	R^2	$1/r^2$
170×20×25	9×9×9	$y=0.0243x^{-0.167}$	0.4924	-0.167
	8×8×8	$y=0.0301x^{-0.444}$	0.9983	-0.444
	7×7×7	$y=0.0220x^{-0.250}$	1	-0.250
170×25×30	9×9×9	$y=0.0232x^{-0.537}$	0.7758	-0.537
	8×8×8	$y=0.0279x^{-0.428}$	0.9926	-0.428
	7×7×7	$y=0.0214x^{-0.259}$	0.9979	-0.259
25×15×20	10×10×10	$y=0.0344x^{-0.963}$	0.9606	-0.963
	9×9×9	$y=0.0341x^{-1.054}$	0.9977	-1.054
	8×8×8	$y=0.0389x^{-0.845}$	0.9652	-0.845
30×20×25	10×10×10	$y=0.0260x^{-0.869}$	0.9664	-0.869
	9×9×9	$y=0.0212x^{-0.593}$	0.9939	-0.593
	8×8×8	$y=0.0198x^{-0.449}$	0.9993	-0.449
35×25×30	10×10×10	$y=0.022x^{-0.230}$	0.9515	-0.230
	9×9×9	$y=0.0199x^{-0.292}$	0.9082	-0.292
	8×8×8	$y=0.0129x^{-0.180}$	0.2028	-0.180

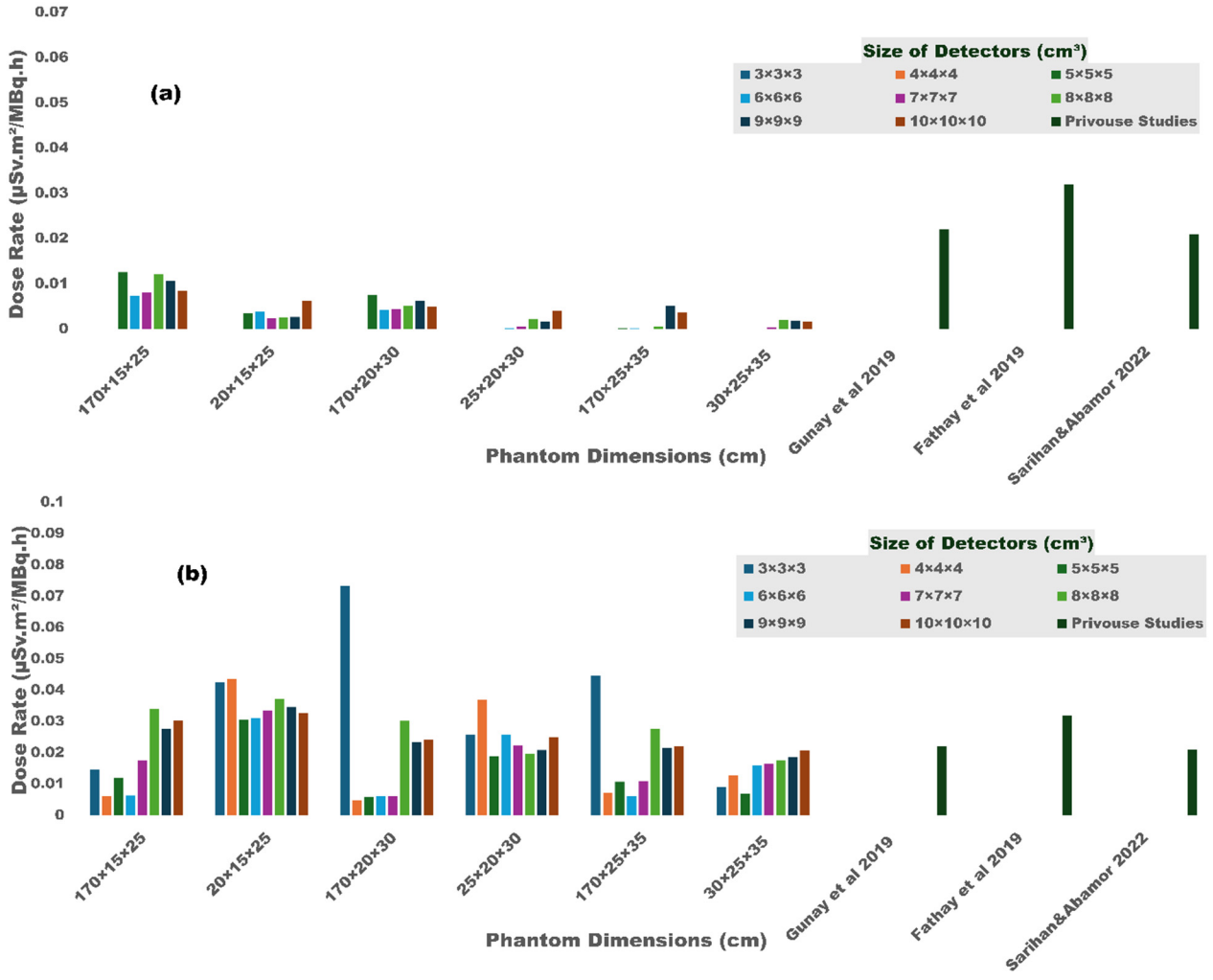

Figure 7. Comparison of Dose rate for the ^{99m}Tc nuclide using (a) Air, (b) Argon detector media for various phantom dimensions and detector sizes at 1 m with previous studies

4. DISCUSSION

This study used MC GATE/Geant4 simulations to calculate the external dose rate constants for six clinically important radionuclides, including ^{99m}Tc, ^{67}Ga, ^{18}F, ^{11}C, ^{131}I, and ^{123}I. The resulting simulated values were compared with three reliable and validated experimental references: Unger & Trubey (1982) [21], Tschurlovits et al. (1992) [23], and Smith & Stabin (2012) [24]. The comparison yielded agreement ratios of 1.089, 1.127, and 1.114, respectively, indicating that all simulation results fell within an acceptable ±10% deviation margin, confirming the accuracy and validity of the MC GATE computational model. This, in turn, indicated good agreement between the MC GATE simulation and

experimentally measured values in radiation dose measurements, reinforcing confidence in computational methods as an effective tool in radiation protection research.

4.1 Influence of Detector Media

The results show a significant correlation between the effective atomic number of the detector media and the sensitivity of the recorded readings, as argon (Z=18) has a larger atomic number than neon (Z=10) and air (Z_{eff}=7.6). On this basis, the argon detector is more efficient than air and neon in absorbing low- and medium-energy photons. Therefore, due to the higher probability that the photoelectric absorption occurs with a higher atomic number, with photon interaction [25].

In contrast, the neon detector failed to record measurable readings, such as T-99m nuclide, and was very low for ^{67}Ga nuclide. As for ^{131}I, the neon detector recorded unexpected readings that were higher than those of the air and argon detectors media. This may be due to the multiple energies of photons. The remaining nuclides recorded readings lower than those of argon and air [26].

The calculated mean dose rate in the presence of the phantom yields the highest value at the argon detector media, followed by air and neon. The neon detector failed to provide any readings for the ^{99m}Tc and ^{123}I nuclides (specifically for the phantom dimension of 35×25×30 cm^3). This is due to the low emission energy of these radionuclides, combined with the low stopping power of neon, leading to insufficient energy deposition within the detector volume with absorption self-attenuation of the phantom [1].

The result shows excellent agreement with previous clinical studies, such as Fathy et al. 2019 [27], in the ^{18}F in an argon detector media; however, for the air detector media, the simulation results showed half the reference value. In the neon media, the reference studies showed higher values than the simulation results.

In contrast, the ^{131}I showed agreement with the reference studies by Fathy et al. 2019 [27] and Al-Esaei et al.2024 [28] across all detector media, particularly for the phantom dimension (25×15×20 cm^3), with perfect agreement. Followed by the ^{67}Ga, which is consistent with the simulation results in the argon media and with the reference studies by Fathy et al. 2019 [27], Fragoso Costa et al. 2021 [29].

Despite the ^{99m}Tc, the air detector media values are significantly lower than those in the reference studies by Fathy et al. 2019 [27], Gunay et al. 2019 [30], and Sarihan & Abamor 2022 [31]. In the argon detector media, however, excellent agreement was observed with the reference studies, in contrast to the neon detector media, which failed to register any readings.

4.2 Influence of Detector Size

The results shown demonstrate that the size of the detector is a decisive factor in measurement accuracy and reading stability, as it can be observed that the dose rate values decrease with an increase in detector size (from 3×3×3 to 10×10×10 cm^3). This phenomenon is physically attributed to the volume averaging effect. Although a larger detector absorbs more total energy, this energy is distributed over a larger mass. Because the regions of the large detector further from the source receive less radiation flux, this spatial averaging reduces the overall recorded dose rate compared to small detectors, which more closely approximate an ideal point-like measurement geometry [26].

In contrast, the simulation data indicates that the dose rate begins to reach a state of stability and convergence at a detector size of (8×8×8 to 10×10×10 cm^3), where it appears that large detectors have a higher stopping power for secondary particles and electrons resulting from the interaction of radiation with the detector media (whether air, argon or neon), as a large detector ensures that majority of secondary particle tracks remain within the volume active, facilitating the establishment of charge particle equilibrium.

4.3 Influence of Phantom Dimensions

The impact of phantom dimensions on the external dose rate was evaluated using different phantom dimensions (20×15×20, 25×20×30, and 30×20×35 cm^3) with detector sizes ranging from (3×3×3 to 10×10×10 cm^3) at 1 m. The results indicate. The increase in phantom dimensions correlates with a gradual decline in the recorded dose rate for all six radionuclides across the various detector media (air, argon, and neon).

Physically, this attenuation is primarily attributed to increased attenuation in tissue-equivalent phantom material. As the dimensions of the phantom increase, the absorption of photons by the phantom before they reach the detector increases, causing a decrease in the observed dose rate [18]. The decrease in the dose rate between the smallest phantom (20×15×25 cm^3) and the largest phantom (30×25×35 cm^3) was approximately 36.8%, indicating that self-attenuation and phantom dimensions reduce the external radiation dose.

The air detector showed lower values than the argon detector, with a total attenuation of 50% for the phantoms. In contrast, the 170 cm long phantoms showed a marked increase in photon attenuation.

Conversely, the results show more stable values for the argon detector, with the small phantoms showing a total attenuation of 37.5%, which is more consistent with previous studies. The large 170 cm phantom also showed a higher degree of photon attenuation compared to the shorter phantom.

These findings reveal that phantom dimensions have a direct effect on workers' radiation exposure. The data suggest that a patient's height, when injected with radioactive pharmaceuticals, is less important than the patient's body thickness,

which is considered the most significant barrier to radiation, and that the patient's height does not affect radiation exposure. This was also confirmed by a Kinsara et al. 2014 study that used MCNP cylindrical phantom shapes of different diameters; it was observed that when the diameters changed, the amount of radiation exposure changed. This was also confirmed by a Kinsara et al. 2014 study that used MCNP cylindrical phantom shapes of different diameters; it was observed that when the diameters changed, the amount of radiation exposure changed [17].

In this context, the use of phantoms with dimensions that differ from the ICRP standard reference phantom, which is based on standardized geometries, is justified; the main reason is that the standard reference phantom is an idealized model, whereas the geometric shapes of patients in nuclear medicine vary and cannot be accurately reflected by the reference phantom. Consequently, the results of this study were designed to assess the extent of variation in phantom dimensions rather than to replace them, and it has been shown that using different phantom dimensions is a valid approach for assessing radiation exposure.

4.4 Influence of Source/Detector distance

As shown, the power-law exponents are highly significant and vary from -0.167 to -1.054 across all phantom configurations studied, in contrast to the theoretical exponent of -2.0 for the inverse-square law. This deviation is ascribed to several major causes, among which the most important that explain the difference in source size between the reconstructed and the real cases are photon attenuation and Compton scattering within the phantom, and effects of source geometry and detector size. The most striking observation is that the phantoms that produced the best values of the coefficient of determination R^2 had exponents that were no closer to the theoretical value of -2.0 for a point source in free space, These results finding the necessity of incorporating realistic phantom geometry and appropriate detector selection into occupational dose assessment for nuclear medicine personnel, rather than relying on simplified point source inverse-square law approximations that may yield inaccurate exposure estimates.. Lastly, these results indicate that argon media can give accurate measurements at 1, 2, and 3 meters.

5. CONCLUSION

This study demonstrated the effectiveness of the MC GATE simulation in calculating external dose rates for the six most important clinical radionuclides used in nuclear medicine: ^{99m}Tc, ^{67}Ga, ^{18}F, ^{11}C, ^{131}I, and ^{123}I. The results were compared with experimental references, and all fell within an acceptable 10± margin of error.

The results confirmed that the argon detector media proved to be the most sensitive and reliable, in contrast to air and neon media, which exhibited unexpected behavior and low sensitivity across the detector size.

Furthermore, detector size was shown to influence the measured response, with dose rate values remaining stable for detector sizes ranging from (8×8×8 to 10×10×10 cm^3), consistent with previous experimental studies.

The simulation results confirmed that phantom dimensions affect radiation exposure, with a mean overall reduction of 36.8% when phantom dimensions were increased from the smallest phantom (25×15×20 cm^3) to the largest phantom (35×25×30 cm^3). In contrast, through various detector media, the actual clinical exposure and how patient-induced exposure reduces occupational exposure for staff. The high-energy emitter radionuclides at 511 keV had the highest radiation exposure: ^{18}F and ^{11}C, followed by ^{67}Ga, ^{131}I, ^{123}I, and lastly ^{99m}Tc.

Conversely, the patient's height is less significant than body thickness, as phantom height does not reduce radiation exposure compared with body thickness, which acts as a physical barrier that reduces occupational exposure for staff. This was analyzed using the inverse-square law, which confirmed the effectiveness of the GATE/Geant4 simulation across various scenarios at different distances and the accuracy of the detector response, with the argon detector media standing out for maintaining readings even at 3 m. Finally, this study presents a reliable computational tool for optimizing external dose rates across various clinical scenarios, providing guidance for improving radiation protection protocols and assessing occupational exposure in nuclear medicine departments.

ORCID

Abdulkhaleq O. Jaralah, https://orcid.org/0009-0006-6399-4657; **Alaa M. Elgohary**, https://orcid.org/0000-0003-4600-6240
Monira M. Rageh, https://orcid.org/0000-0002-2350-6595; **Magdy M. Khalil**, https://orcid.org/0000-0003-2087-5229

REFERENCE

[1] M.M. Khalil, Basic *Sciences of Nuclear Medicine* (Springer International Publishing, Cham, 2021).
[2] M.M. Khalil, Basic *Science of PET Imaging* (Springer International Publishing, Cham, 2017).
[3] M.U. Khan, and M.S. Usmani, "Radionuclide Infection Imaging: Conventional to Hybrid," in: *12 Chapters on Nuclear Medicine*, (IntechOpen, 2011).
[4] R.J. Groper, D.K. Glover, and A.J. Sinusas, *Cardiovascular Molecular Imaging* (CRC Press, Boca Raton, 2007). https://doi.org/10.3109/9781420005097
[5] H.R. Maxon, and H.S. Smith, "Radioiodine-131 in the diagnosis and treatment of metastatic well differentiated thyroid cancer," *Endocrinol. Metab. Clin. North. Am.* **19**(3), 685–718 (1990).
[6] X. Deng, J. Rong, L. Wang, N. Vasdev, L. Zhang, L. Josephson, and S.H. Liang, "Chemistry for Positron Emission Tomography: Recent Advances in 11 C-, 18 F-, 13 N-, and 15 O-Labeling Reactions," *Angw. Chem*. **58**(9), 2580–2605 (2019). https://doi.org/10.1002/anie.201805501

[7] S.Y. Ho, and D.R. Shearer, "Radioactive contamination in hospitals from nuclear medicine patients," *Health Physics*, **62**(5), 462-466 (1992). https://doi.org/10.1097/00004032-199205000-00015
[8] F. Jafarian-Dehkordi, and C. Hoeschen, "Low-Dose radiation risk in medicine: a look at risk models, challenges, and future prospects," Z. Med. Phys. **35**(4), 393–400, (2025). https://doi.org/10.1016/j.zemedi.2025.07.002
[9] IAEA, *Occupational Radiation Protection: General Safety Guide*, (International Atomic Energy Agency, Vienna, 2018).
[10] IAEA, *ORPGUIDE: Occupational radiation protection; IAEA safety standards series*, (International Atomic Energy Agency, Vienna, 2000).
[11] ICRP. "The 2007 Recommendations of the International Commission on Radiological Protection. ICRP publication 103," Ann. ICRP **37**(2-4), 1–332 (2007). https://doi.org/10.1016/j.icrp.2007.10.003
[12] M. Abuqbeitah, M. Demir, I. Çavdar, H. Tanyildizi, N. Yeyin, L. Uslu-Beşli, L. Kabasakal, *et al*., "Red bone marrow dose estimation using several internal dosimetry models for prospective dosimetry-oriented radioiodine therapy," Radiat. Environ. Biophys. **57**(4), 395–404 (2018). https://doi.org/10.1007/s00411-018-0757-2
[13] L.K. Harding, N.J. Harding, H. Warren, A. Mills, and W.H. Thomson, "The radiation dose to accompanying nurses, relatives and other patients in a nuclear medicine department waiting room," Nucl. Med. Commun. **11**(1), 17–22 (1990). https://doi.org/10.1097/00006231-199001000-00004
[14] N. Sirag, and A. Elrazek, "Design considerations to minimize staff doses in nuclear medicine units," Int. J. Eng. Tech. Res. **4**(1), 226–245 (2015).
[15] D. Visvikis, M. Bardies, S. Chiavassa, C. Danford, A. Kirov, F. Lamare, L. Maigne, *et al*., "Use of the GATE Monte Carlo package for dosimetry applications," Nucl. Instrum. Methods Phys. Res., Sect. A, **569**(2), 335–340 (2006). https://doi.org/10.1016/j.nima.2006.08.049
[16] J. Ierace, P. Rowshanfarzad, C. Sinnott, R. Nezich, P. Brayshaw, and M. Djukelic, "From Point Sources to Phantoms: Refining Dose Rate Models in Nuclear Medicine with Tc-99m, F-18, I-131 and Lu- 177," Physical and Engineering Sciences in Medicine, preprint (2025). https://doi.org/10.21203/rs.3.rs-7707816/v1
[17] A. Kinsara, S. Abdul-Majid, W. El-gammal, T. Albaghdadi, A. Maimani, and W. Abulfaraj, "External radiation doses from patients administered with radiopharmaceuticals measurements and Monte Carlo simulation," Nucl. Technol. Radiat. Prot. **29**, 199–206 (2014). https://doi.org/10.2298/NTRP1403199K
[18] A. D. Soares, L. Paixão, and A. Facure, "Determination of the dose rate constant through Monte Carlo simulations with voxel phantoms," Med. Phys. **45**(11), 5283–5292 (2018). https://doi.org/10.1002/mp.13181
[19] J. Allison, *et al*., "Recent developments in Geant4," Nucl. Instrum. Methods Phys. Res., Sect. A, **835**, 186–225 (2016). https://doi.org/10.1016/j.nima.2016.06.125
[20] E. N. Obikili, and A. B. Okesina, "Transverse thoracic diameter in frontal chest radiographs of an adult Nigerian population," West Afr. J. Med. **25**(3), 186–189 (2007). https://doi.org/10.4314/wajm.v25i3.28275
[21] L. M.Unger, and D. K. Trubey, *Specific gamma-ray dose constants for nuclides important to dosimetry and radiological assessment*, (Oak Ridge Nat. Lab. Radiat. Shielding Inform. Cent., Oak Ridge, TN, 1982).
[22] OpenGATE Collaboration, Tools to Interact with the Simulation: Actors (GATE Documentation, 2026).
[23] M. Tschurlovits, A. Leitner, and G. Daverda, "Dose Rate Constants for New Dose Quantities," Radiat. Prot. Dosim. **42**(2), 77–82 (1992). https://doi.org/10.1093/oxfordjournals.rpd.a081281
[24] D. S.Smith, and M. G. Stabin, "Exposure rate constants and lead shielding values for over 1,100 radionuclides," Health Phys. **102**(3), 271–291 (2012). https://doi.org/10.1097/HP.0b013e318235153a
[25] D.W.O. Rogers, "Introduction to Radiological Physics and Radiation Dosimetry by F. H. Attix," Med. Phys. **14**(4), 692 (1987). https://doi.org/10.1118/1.596041
[26] G. F. Knoll, *Radiation detection and measurement*, (John Wiley & Sons, 2010).
[27] M. Fathy, M. M. Khalil, W. M. Elshemey, and H. S. Mohamed, "Occupational radiation dose to nuclear medicine staff due to Tc99m, F18-FDG PET and therapeutic I-131 based examinations,"" Radiat. Prot. Dosim. **186**(4), 443–451 (2019). https://doi.org/10.1093/rpd/ncz046
[28] A. Al-Esaei, E. Saleh, S. Maghraby, T. Elsayed, and T. Kany, "Evaluation of Radiation Safety Parameters from Patients Receiving I-131 Therapy for Thyroid Carcinoma," J. Med. Phys. Appl. Sci. **9**(1), 52 (2024). https://doi.org/10.36648/2574-285x.9.1.52
[29] P. F. Costa, *et al*., "Radiation Protection and Occupational Exposure on 68Ga-PSMA-11–Based Cerenkov Luminescence Imaging Procedures in Robot-Assisted Prostatectomy," J. Nucl. Med. **63**(9), 1349–1356 (2022). https://doi.org/10.2967/jnumed.121.263175
[30] O. Günay, M. Sarıhan, O. Yarar, *et al*., "Determination of radiation dose from patients undergoing Tc-99m Sestamibi nuclear cardiac imaging," Int. J. Environ. Sci. Technol. **16**, 5251–5258 (2019). https://doi.org/10.1007/s13762-019-02262-1
[31] M. Sarihan, and E. Abamor, "Radiation dose measurement on bone scintigraphy and planning clinical management," Open Phys. **20**(1), 1176–1184 (2022). https://doi.org/10.1515/phys-2022-0211

ОЦІНКА ПОТУЖНОСТІ ГАММА-ОПРОМІНЮВАННЯ ДЛЯ КЛІНІЧНО ЗНАЧНИХ РАДІОНУКЛІДІВ У ЯДЕРНІЙ МЕДИЦИНІ З ВИКОРИСТАННЯМ МОДЕЛЮВАННЯ МОНТЕ-КАРЛО GATE/GEANT4

Абдулхалек О. Джаралах[1], Алаа М. Елгохарі[1], Моніра М. Рагех[1], Магді М. Халіл[2,3]
[1]Кафедра біофізики, факультет природничих наук, Каїрський університет, Єгипет
[2]Медична біофізика, кафедра фізики, факультет природничих наук, Хелуанський університет
[3]Школа прикладних медичних наук, Університет Бадр у Каїрі (BUC), Каїр, Єгипет

Мета. Розробити надійний обчислювальний метод для розрахунку потужності дози зовнішнього опромінення пацієнтів ядерної медицини за допомогою моделювання методом Монте-Карло та систематично оцінити вплив геометрії фантома й характеристик детектора на професійне опромінення. **Методи:** Моделювання MC GATE версії 9.1 (Geant4 10.7) розрахувало

константи потужності зовнішньої дози для більшості клінічних радіонуклідів: ^{99m}Tc, ^{67}Ga, ^{18}F, ^{11}C, ^{131}I та ^{123}I. Було використано два фантоми: один із розмірами (25×15×20, 30×20×25 та 35×25×30 см³), а інший — з фіксованою довжиною 170 см та змінною шириною (15×20, 20×25 та 25×30 см³), специфічними для нукліда ^{99m}Tc. Розміри детекторів (від 3×3×3 до 10×10×10 см³) оцінювалися на відстанях 1, 2 та 3 м. Різні середовища детектора (повітря, аргон та неон) оцінювалися на чутливість до фотонів. Результати порівнювали з експериментальними даними. **Результати:** Результати моделювання узгоджувалися з експериментальними даними в межах ±10%. Аргон продемонстрував вищу чутливість порівняно з повітряними і неоновими середовищами детектора. Розміри фантома загалом збільшилися, що призвело до зменшення самозатухання на 36,8%. Радіонукліди ^{18}F та ^{11}C, а також ^{67}Ga, ^{131}I, ^{123}I та ^{99m}Tc, становили найбільшу небезпеку професійного опромінення. Товщина тіла пацієнта була більш значним фактором ослаблення, ніж його зріст. **Висновок:** Моделювання GATE/Geant4 забезпечує надійний і точний інструмент для оцінки потужності зовнішньої дози у відділеннях ядерної медицини. Ці результати підкреслюють важливість використання відповідних розмірів детекторів і середовищ, а також реалістичної геометрії пацієнта в оцінці професійної дози та надають важливі дані для вдосконалення протоколів радіаційного захисту.

Ключові слова: *потужність зовнішньої дози; ядерна медицина; радіаційний захист; моделювання методом Монте-Карло; константа швидкості гамма-випромінювання*